Journal of *Marine Science and Engineering*

MDPI

Article

Biological and Proteomic Characterization of the Anti-Cancer Potency of Aqueous Extracts from Cell-Free Coelomic Fluid of *Arbacia lixula* Sea Urchin in an In Vitro Model of Human Hepatocellular Carcinoma

Claudio Luparello [1,*], Rossella Branni [1], Giulia Abruscato [1], Valentina Lazzara [1], Simon Sugár [2], Vincenzo Arizza [1], Manuela Mauro [1], Vita Di Stefano [1] and Mirella Vazzana [1]

[1] Dipartimento di Scienze e Tecnologie Biologiche, Chimiche e Farmaceutiche (STEBICEF), Università Di Palermo, Viale Delle Scienze, 90128 Palermo, Italy
[2] MS Proteomics Research Group, Research Centre for Natural Sciences, Eötvös Loránd Research Network, 1117 Budapest, Hungary
* Correspondence: claudio.luparello@unipa.it; Tel.: +39-91-238-97405

Abstract: Echinoderms are an acknowledged source of bioactive compounds exerting various beneficial effects on human health. Here, we examined the potential in vitro anti-hepatocarcinoma effects of aqueous extracts of the cell-free coelomic fluid obtained from the sea urchin *Arbacia lixula* using the HepG2 cell line as a model system. This was accomplished by employing a combination of colorimetric, microscopic and flow cytometric assays to determine cell viability, cell cycle distribution, the possible onset of apoptosis, the accumulation rate of acidic vesicular organelles, mitochondrial polarization, cell redox state and cell locomotory ability. The obtained data show that exposed HepG2 cells underwent inhibition of cell viability with impairment of cell cycle progress coupled to the onset of apoptotic death, the induction of mitochondrial depolarization, the inhibition of reactive oxygen species production and acidic vesicular organelle accumulation, and the block of cell motile attitude. We also performed a proteomic analysis of the coelomic fluid extract identifying a number of proteins that are plausibly responsible for anti-cancer effects. Therefore, the anti-hepatocarcinoma potentiality of *A. lixula*'s preparation can be taken into consideration for further studies aimed at the characterization of the molecular mechanism of cytotoxicity and the development of novel prevention and/or treatment agents.

Keywords: coelomic fluid; sea urchin; echinoderm; HepG2 cells; apoptosis; cell cycle; acidic vesicular organelles; mitochondrial transmembrane potential; reactive oxygen species; wound healing assay

Citation: Luparello, C.; Branni, R.; Abruscato, G.; Lazzara, V.; Sugár, S.; Arizza, V.; Mauro, M.; Di Stefano, V.; Vazzana, M. Biological and Proteomic Characterization of the Anti-Cancer Potency of Aqueous Extracts from Cell-Free Coelomic Fluid of *Arbacia lixula* Sea Urchin in an In Vitro Model of Human Hepatocellular Carcinoma. *J. Mar. Sci. Eng.* **2022**, *10*, 1292. https://doi.org/10.3390/jmse10091292

Academic Editor: Alexandre Lobo-da-Cunha

Received: 28 July 2022
Accepted: 9 September 2022
Published: 13 September 2022

1. Introduction

The marine environment, which occurs in about 70% of the globe's surface and 90% of the biosphere, is the largest habitat of the Earth. It harbors a significant fraction of the world's biodiversity with many still unknown species and represents a little exploited treasure chest rich in bioactive natural products. In fact, animal adaptation processes to the different and often extreme aquatic environments have led to the establishment of unique bio-synthetic pathways [1]. Within this context, the development of interindividual signalization systems and defensive strategies, e.g., against predators, infectious agents and UV radiations, prompted sessile aquatic species to set up networks of chemical communication through a variety of exclusive marine species-specific metabolites, which can be available for extraction and characterization as a massive library of natural active compounds [2,3].

One of the acknowledged potential applications shared among several marine natural products is related to cancer prevention and treatment. Studies performed on compounds extracted from sponges, mollusks, soft corals and tunicates demonstrated their relevant

cytotoxic and anti-tumoral properties against different human cancer cell lines in vitro, also acting upon disparate cellular functions such as locomotory ability, gene expression reprogramming and autophagic flux [4–8]. Notably, based on their pharmacological properties and added health benefits, marine bioactives are increasingly considered promising additives for the development of functional foods and active food-packaging material [9–11].

Among the marine invertebrates, the phylum Echinodermata (Klein, 1778) is widely distributed worldwide, consisting of about 7000 extant species grouped into five well-defined taxonomic classes. The non-edible sea urchin *Arbacia lixula* (Linnaeus, 1758; Echinoidea, Arbacioida: Arbaciidae), which colonized the Mediterranean shallow rocks during the Pleistocene [12], is a warm-temperate water organism that has been used as a model for chemical embryotoxicity studies and to determine the effects of high-frequency noises on the immune response [13–15]. The data dealing with the biomedical applications of *A. lixula*'s components are limited to date. In this regard, *A. lixula*'s eggs have been proven as a valuable source of the free radical scavenger astaxanthin, whereas its coelomic fluid and the cells contained therein were found to possess a strong anti-oxidant activity [16–18]. In addition, potentially anti-microbial peptides were also identified in the coelomic fluid of this organism [19].

We previously demonstrated that the cell-free coelomic fluid extract (CFE) obtained from this species is able to exert cytotoxic effects against triple-negative breast cancer cells in culture [20], thus prompting the extension of such in vitro trials also to other tumor cell model systems. The physiological benefits of potential additives for functional foods or food-packaging purposes include the maintenance of the health of the organs of the digestive apparatus. Thus, we chose to expand the knowledge on the potential anti-tumoral effects of *A. lixula*'s CFE by focusing our interest on an in vitro model system representative of tumor-affected liver parenchyma. For this purpose, we studied the biological effects exerted on the HepG2 cell line derived from liver biopsies of a 15-year-old Caucasian male suffering from a differentiated hepatocellular carcinoma [21]. It is widely acknowledged that the proper characterization of the biological activity of new potential anti-cancer products is valuable to establish their efficacy profiles and discover new applications. Moreover, information on their mechanisms of action may reveal new molecular targets of beneficial effect, ultimately serving as a link to clinical activity by designing appropriate interventions and therapies for specific tumor cytotypes [22]. Therefore, the aim of our investigation was to examine the CFE-mediated effects on cell viability and to obtain more insight into the intracellular mechanisms of cytotoxic induction by employing a combination of colorimetric, microscopic and flow cytometric assays to determine cell cycle distribution, the possible onset of apoptosis, the accumulation rate of acidic vesicular organelles (AVOs), mitochondrial polarization and cell redox state and cell locomotory ability. The obtained data show that the CFE treatment of HepG2 cells caused the inhibition of cell viability with impairment of cell cycle progress coupled to the onset of apoptotic death, the induction of mitochondrial depolarization, the inhibition of reactive oxygen species (ROS) production and AVO accumulation, and the impairment of cell motile attitude. As a complement to the phenotypic characterization, the data obtained from the proteomic analysis of the CFE identified a number of proteins plausibly responsible for the observed impairment of biological activity in HepG2 cells.

2. Materials and Methods

2.1. Catching and Maintaining the Animals

A total of 60 individuals of sea urchins of the species *A. lixula* (Figure 1) were collected from the rocky coves of the Gulf of Palermo (Sicily, Italy) at a depth of 5–10 m. Before starting the experiments, the animals were acclimatized in aquaria for two weeks in recirculated and filtered artificial seawater (9 mM KCl; 0.425 M NaCl; 0.0255 M $MgSO_4 \cdot 7H_2O$; 9.3 mM $CaCl_2 \cdot 2H_2O$; 0.023 M $MgCl_2 \cdot 6H_2O$; 2 mM $NaHCO_3$, pH 8.0) at 15 ± 2 °C with constant flow-through of dissolved O_2 and fed with commercially available invertebrate food (Algamac 3000, Aquafauna Bio-Marine Inc., Hawthorne, CA, USA).

Figure 1. An *A. lixula* sea urchin specimen.

2.2. Bleeding Procedure and Preparation of the CFE

As already reported by Luparello et al. [23], the CF was collected by cutting the peristomial membrane of the sea urchins and harvesting the bleeding fluid in the presence of cold 60ISO-EDTA anticoagulant (20 mM Tris, 0.5 mM NaCl, 70 mM EDTA; pH 7.5). The CF was immediately centrifuged at 1000× *g* for 10 min at 4 °C to obtain a cell-free extract, which was stored at −80 °C and subsequently lyophilized in an Alpha 2–4 LD plus freeze-dryer (Martin Christ, Osterode am Harz, D). The lyophilized sample was resuspended in the minimum volume of sterile distilled water and kept at −20 °C until used for the cytotoxicity assays. The protein concentration of the CFE was determined using the Qubit Protein Assay Kit in a Qubit 3.0 fluorometer (Thermo Fisher, Waltham, MA, USA), according to the manufacturer's instructions.

2.3. Proteomic Analysis

The proteomic analysis was performed as reported elsewhere [23], including sample preparation, liquid chromatography–mass spectrometry (HPLC-MS) analysis and protein identification. Briefly, the proteins in the sample were reduced using RapiGest and dithiothreitol (Thermo Fisher), then alkylated using iodoacetamide (Thermo Fisher) and finally digested using LysC-Trypsin and Trypsin (Mass Spec grade, Promega, Madison, WI, USA) in two-steps. After proteolysis was stopped by adding formic acid (Thermo Fisher), the samples were dried and desalted using C18 spin columns (Thermo Fisher). The samples were stored at −20 °C until the analysis. A total nominal amount of 1.5 µg protein was then analyzed from each sample using a Dionex Ultimate 3000 nanoRSLC (Dionex, Sunnyvale, CA, USA) system coupled to a Bruker Maxis II ETD mass spectrometer (Bruker Daltonics GmbH, Bremen, D) via a CaptiveSpray nanobooster ion source. For peptide separation, an ACQUITY UPLC M-Class Peptide BEH C18 column (Waters, Milford, MA, USA) was used. Proteins were identified by searching against the Uniprot Aechinodermata database using the Byonic (v4.2.10, Protein Metrics Inc., Cupertino, CA, USA) software search engine. Protein hits were further filtered by Scaffold (version 4.11, Proteome Software, Inc., Portland, OR, USA). Quantitative proteomic information was provided by Scaffold's quantitative analysis. Subsequently, protein identification was also performed by BlastP comparison to the non-redundant protein sequence database (available at https://blast.ncbi.nlm.nih.gov/Blast.cgi?PAGE=Proteins; accessed on 1 May 2022). An expected value <1 was set as the cutoff.

2.4. Cell Cultures

HepG2 hepatocellular carcinoma cells, taken from laboratory stocks, were grown in D-MEM medium (Sigma, St. Louis, MO, USA) plus 10% fetal calf serum (FCS; Thermo Fisher, Waltham, MA, USA) and antibiotics (100 U/mL penicillin and 100 µg/mL streptomycin; Thermo Fisher, Waltham, MA, USA), at 37 °C in a 5% CO_2 atmosphere.

2.5. Viability Assays

An MTT assay was performed to evaluate cell viability under control and treated conditions [24]. Briefly, after plating at a concentration of 5500 cells/well in 96-well plates and overnight adhesion, HepG2 cells were exposed for 24 or 48 h to the CFE at 2.5, 5, 10 or 15 µg/mL concentrations. After the addition of MTT and the incubation with the solubilization buffer, the absorbance of the solubilized formazan was evaluated in an automated microplate reader at a λ = 550 nm. After calculation of the viability ratio between treated and control cells, the half maximal inhibitory concentration (IC_{50}) at 24 h (IC_{50}24) and 48 h (IC_{50}48) was evaluated with the online calculator available at https://www.aatbio.com/tools/ic50-calculator (accessed on 6 March 2021). The subsequent biological assays were performed, exposing cells to either the IC_{50}24 or the IC_{50}48 of the CFE for 24 or 48 h, respectively.

In parallel experiments, HepG2 cells were co-treated with 1 nM rapamycin (Sigma), a macrolide antibiotic functioning as an autophagy activator [25] and IC_{50} of the CFE for 24 h. The reversion of the cytotoxic effect, if any, was monitored through the trypan blue exclusion test. DMSO-treated cells were used as controls.

2.6. Wound Healing Assay

The scratch/wound healing assay, commonly used to study the cell motile attitude in vitro, was performed according to [23]. Briefly, HepG2 cells were seeded in 6-well plates and allowed to form a sub-confluent monolayer. Then, after the cell layer was scraped three times in parallel with a 200 µL pipette tip and a perpendicular line was drawn with a permanent marker, the culture medium was replaced with either an unsupplemented medium (control sample) or medium containing the CFE at the IC_{50}24 (treated sample). Selected sites of intersection between the scratched monolayer and the drawn line were photographed under a phase-contrast microscope at fixed time intervals in the 24 h following the beginning of the assay. The quantification of the wound area was performed using the ImageJ/Fiji® plug-in.

2.7. Flow Cytometry Assays

For each of the following analyses, three independent assays were performed as described in [20,23,26,27] using a FACSCanto flow cytometer (BD Biosciences, Franklin Lakes, NJ, USA) and evaluating 10,000 events. The resulting fcs files were processed with the Floreada analysis tool available at https://floreada.io (accessed on 1 April 2022). In order to exclude debris, which displayed low FSC values, from the analyses, gating in the FSC vs. SSC plot was performed for every determination. Moreover, gating in the FSC-H vs. FSC-A plot was also performed to exclude doublets and multiplets in cell cycle analyses.

2.7.1. Cell Cycle Distribution Assay

Cell cycle distribution was determined by fixation of control and exposed cells with cold 70% ethanol, incubation with 40 µg RNAse A/mL and final staining with 20 µg propidium iodide/mL before the flow cytometrical analysis.

2.7.2. Apoptosis Assay

The percentage of apoptotic cells under control and exposed preparations was evaluated using the Annexin V-FITC kit (Canvax Biotech, Cordoba, Spain), following the manufacturer's instructions.

2.7.3. Analysis of Mitochondrial Transmembrane Potential (MMP)

The MMP state was examined using the dye JC1 (Molecular Probes, Eugene, OR, USA), which exhibits potential-dependent accumulation and a fluorescence emission shift from green (~529 nm) to red (~590 nm) in intact mitochondria whereas, in the case of dissipated MMP, a decrease in the red/green fluorescence intensity ratio occurs. In parallel with

the negative controls and CFE-treated samples, HepG2 cells were also exposed to 1 μM valinomycin, an MMP loss-inducer K+ ionophore, as a positive control.

2.7.4. ROS Assay

The extent of intracellular ROS production was evaluated using the ROS Detection Assay Kit (Canvax Biotech, Cordoba, Spain) according to the manufacturer's instructions.

2.7.5. AVO Accumulation Assay

The extent of AVO accumulation was examined by fixing control and treated cells with cold 70% ethanol and staining with 100 μg acridine orange/mL (Sigma) for 20 min in the dark before the flow cytometric analysis.

2.8. Statistics

The analysis of variance (ANOVA) tests was performed with SigmaPlot 11.0 software (SYSTAT, San Jose, CA, USA). A p-value < 0.05 was considered statistically significant.

3. Results

In the first set of assays, we examined the effect exerted by exposure to *A. lixula*'s CFE on HepG2 cells' survival via an MTT assay. As shown in Figure 2, cell exposure for 24 or 48 h to either preparation caused a dose-dependent decrease in cell viability with an average $IC_{50}24$ of 15.7 μg/mL and $IC_{50}48$ of 7.45 μg/mL, respectively. These IC_{50} concentrations were used in the subsequent analyses, which aimed to gather more detailed data on the subcellular aspects of CFE-induced toxicity on HepG2 cells via a panel of flow cytometric assays.

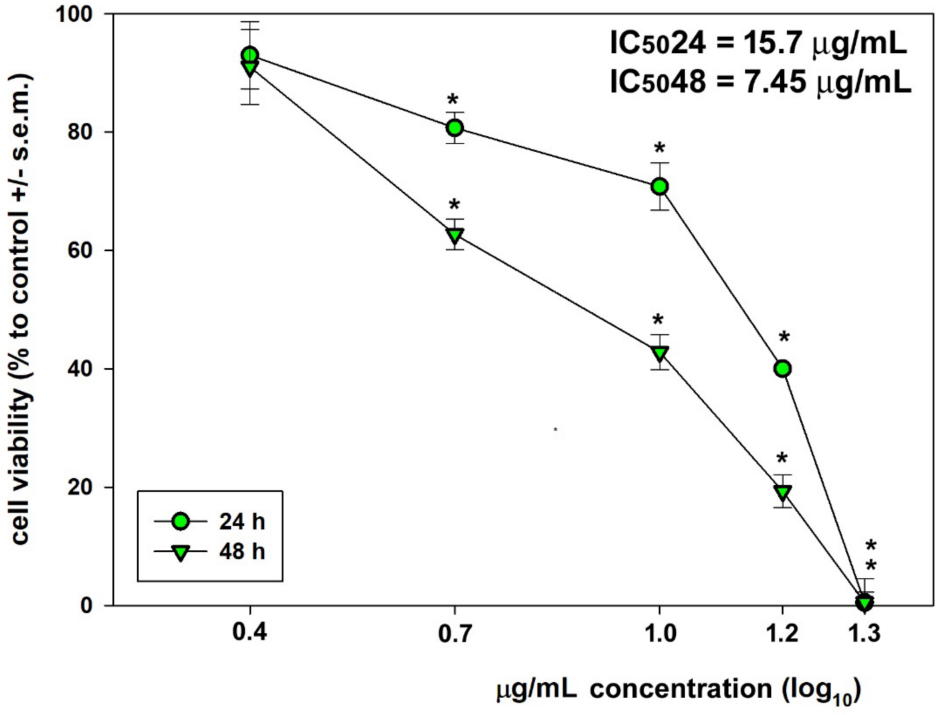

Figure 2. Dose-response effect of the CFE from *A. lixula* at 2.5, 5, 10 and 15 μg/mL concentration on the viability of HepG2 after either 24 or 48 h of exposure. The error bars correspond to the standard error of the mean (s.e.m.) of three independent measurements. * p < 0.05.

We initially examined which kind of perturbation of the cell cycle progress could be found after treatment with the preparation. For this purpose, HepG2 cells exposed to the $IC_{50}24$ or $IC_{50}48$ of the CFE were stained with propidium iodide (PI) and submitted

to flow cytometric analysis of the distribution of cell population in the cycle phases. As shown in Figure 3, if compared to controls, the result of 24 h of exposure to the extracts was a decrease in the proportion of cells in the G_0/G_1 phase fraction (average control vs. CFE = 47.4% vs. 29.72%), and an increase in the cell percentages in the sub-G_0 fractions (average control vs. CFE = 8.4% vs. 26.18%). No significant change was observed for the other cell cycle phases. Only a progressive increase in the sub-G_0 fraction could be observed at earlier times, i.e., 2 and 4 h (not shown). In addition, cell treatments with the $IC_{50}48$ of the CFE for 48 h determined a generalized decrease in all the cell percentages in the cycle phases and a further increase in the sub-G_0 fraction, thus indicating the generalized exacerbation of the cell cycle arrest and the induction of cell death as results of the longer-term exposure.

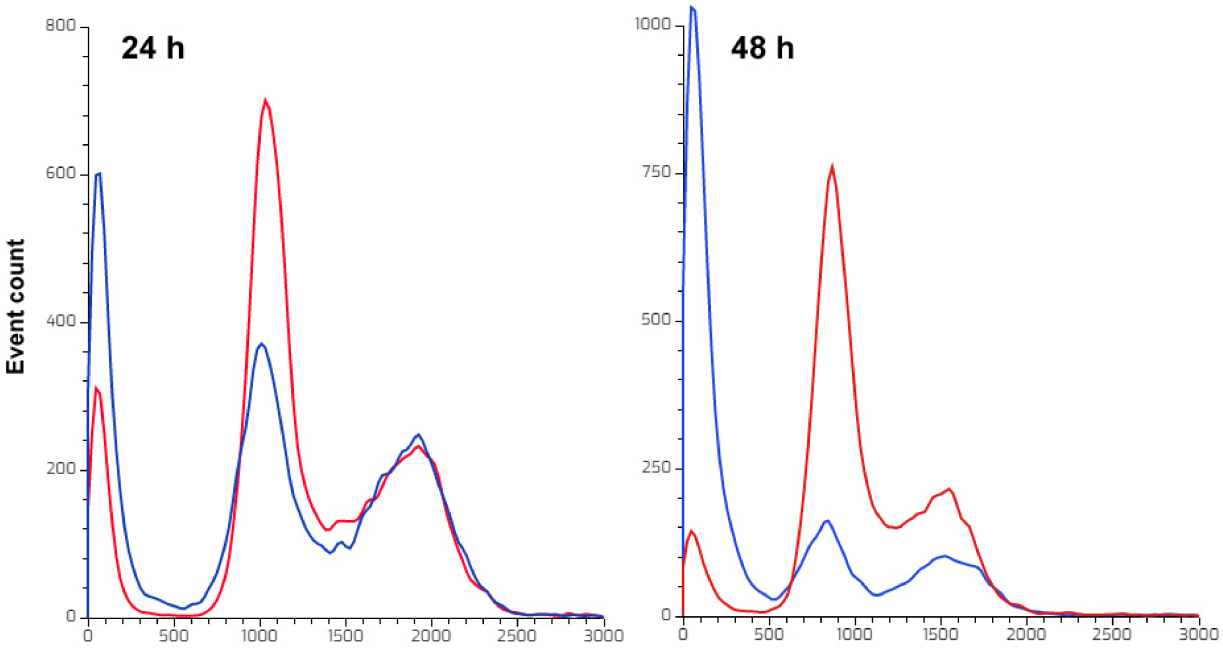

	control	treated
subG₀	10.06 +/- 1.1%	26.18 +/- 3.13%
G₀/G₁	46.08 +/- 3.16%	29.72 +/- 2.29%
S	13.37 +/- 3.25%	13.45 +/- 1.5%
G₂/M	30.98 +/- 1.71%	30.01 +/- 1.24%

	control	treated
subG₀	6.72 +/- 0.13%	74.5 +/- 8.86%
G₀/G₁	48.79 +/- 1.59%	8.74 +/- 3.49%
S	13.37 +/- 3.25%	2.7 +/- 0.82%
G₂/M	30.98 +/- 1.71%	13.89 +/- 4.62%

Figure 3. Representative DNA profiles of control (red line) and CFE-treated (blue line) HepG2 cells after 24 and 48 h of exposure. The cell population distribution in the cycle phases in triplicate experiments is reported in the annexed panels as the mean ± s.e.m.

Based on the accumulation of HepG2 cells treated with $IC_{50}24$ CFE for 24 h in the sub-G_0 phase fraction, indicative of the occurrence of DNA fragmentation ascribable to the onset of necrosis and/or apoptosis, the tumor cells were submitted to annexin V-FITC/PI staining with the aim to determine the possible externalization of phosphatidylserine, a hallmark of apoptosis promotion. On the one hand, the obtained results, shown in Figure 4, demonstrate that the percentage of the viable annexin-V^-/PI^- cells decreased from about 84% of the controls to about 56% after the treatment. On the other hand, the percentage of late apoptotic cells (annexin-V^+/PI^+) increased from about 14% of the controls to about 41%. This result is in accordance with the previous data regarding the increasing amount of the sub-G_0 cell population already at 24 h of exposure to the CFE. No significant difference was found between the necrotic, i.e., annexin-V^-/PI^+, cell populations in the two experimental conditions.

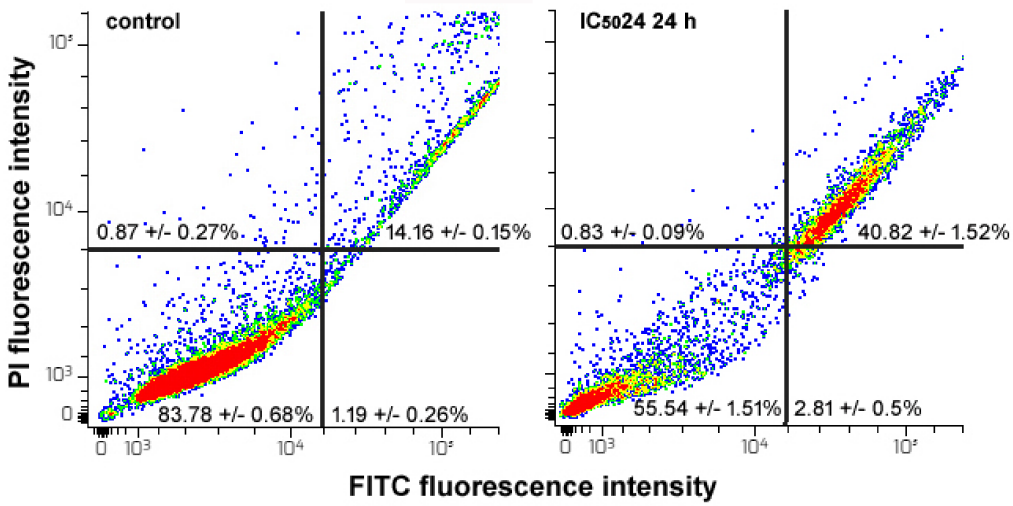

Figure 4. Flow cytometric assays for apoptosis in HepG2 cells cultured under control conditions or exposed to CFE $IC_{50}24$ for 24 h. The plots show the results of representative experiments, and the percentages indicated as the mean ± s.e.m. of three independent experiments refer to viable annexin-V^-/PI^- cells (bottom left quadrant), early apoptotic annexin-V^+/PI^- cells (bottom right quadrant), late apoptotic annexin-V^+/PI^+ cells (top right quadrant) and necrotic annexin-V^-/PI^+ cells (top left quadrant).

Then, we determined whether cell exposure to the extract could impair the mitochondrial function by monitoring mitochondrial polarization status with the membrane-permeable JC1 dye, which is sensitive to changes in the MMP, thereby evaluating the percentage of cells with bright green/bright red emission (indicative of intact MMP) and of those ones with bright green/dim red emission (indicative of MMP collapse). Figure 5 shows that the CFE determined the dissipation of the MMP. In particular, after 24 h and 48 h of exposure to the preparations at the $IC_{50}24$ and $IC_{50}48$, the dim red-emitting cells were found to increase from about 27% and 25% of the controls to about 48% and 98%, respectively. In the latter case, the value obtained was coincident with that of the positive control treated for 48 h with valinomycin.

The ability of the CFE to dysregulate mitochondrial metabolism was also investigated through the evaluation of the accumulation of ROS. The produced amount of peroxide-like and nitric oxide-derived reactive molecules was monitored by flow cytometric analysis of the oxidation extent of the H_2DCFDA probe to green-emitting DCF at early (4 h of exposure) and late (24 h of exposure) time points. By analogy with other experimental models [23,28–30], two distinct cell subpopulations endowed with low (ROS^-) and high rates (ROS^+) of ROS generation were found in each sample. Thus, we evaluated the mean fluorescence intensity (MFI) of the events associated with the ROS^+ subpopulations in the different experimental conditions to compare their rates. The results obtained show the occurrence of a drastic down-regulation of ROS generation after short-term incubation with the CFE (average control cells' MFI vs. treated cells' MFI = 11,662 vs. 2885), which remained approximately constant after 24 h of exposure (average MFI = 2064) although a decrease in ROS accumulation could be observed at this time point also under control conditions (average MFI = 6710) (Figure 6). As reported by Raja et al. [29], we also evaluated the ratio between ROS^+ and ROS^- cells within the whole population. As shown in Figure 7, CFE treatment correlated with very low levels of basal ROS (average control cells' ratio vs. treated cells' ratio = 1.39 vs. 0.18 at 4 h and 8.73 vs. 0.07 at 24 h). Cumulatively, the obtained data are consistent with the idea that the switching-off of ROS production contributes to the cytotoxic activity of the CFE.

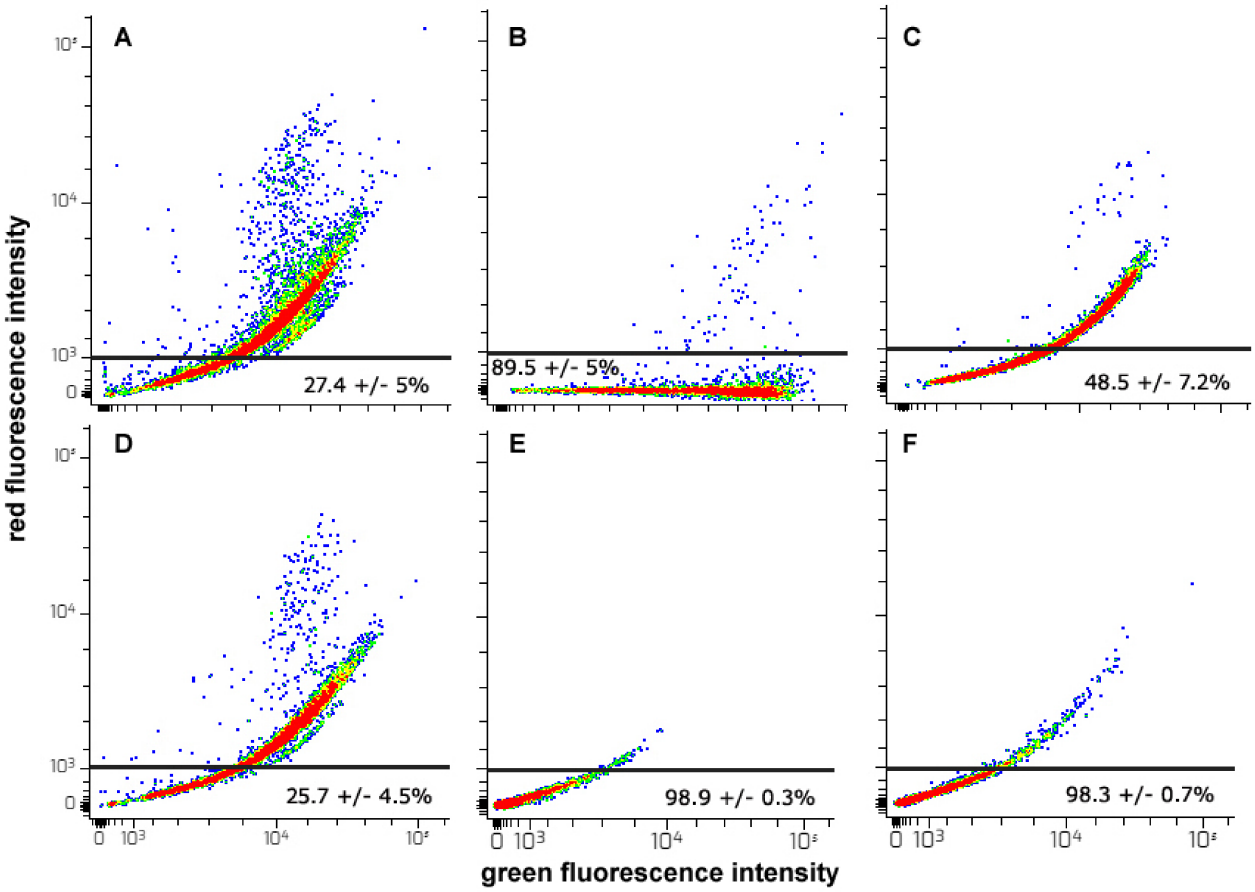

Figure 5. Flow cytometric assays for MMP in HepG2 cells cultured for 24 (**A**–**C**) or 48 h (**D**–**F**) under control conditions (**A**,**D**), in the presence of 1µM valinomycin (**B**,**E**) and of either CFE IC_{50}24 (**C**) or CFE IC_{50}48 (**F**). The plots display the outputs of representative experiments, and the percentages in the bottom quadrants of each frame expressed as the mean ± s.e.m. of triplicate experiments are related to dim red-emitting cells that underwent collapse of MMP.

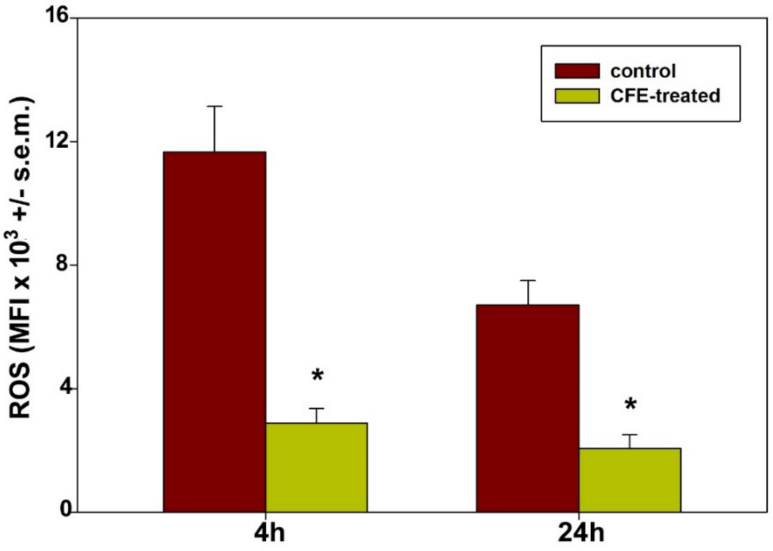

Figure 6. Bar graphs showing the ROS-associated MFI in ROS^+ cell subpopulations of control and IC_{50}24 CFE-treated HepG2 cells for 4 and 24 h. The error bars correspond to the standard error of the mean (s.e.m.) of three independent measurements. * $p < 0.05$.

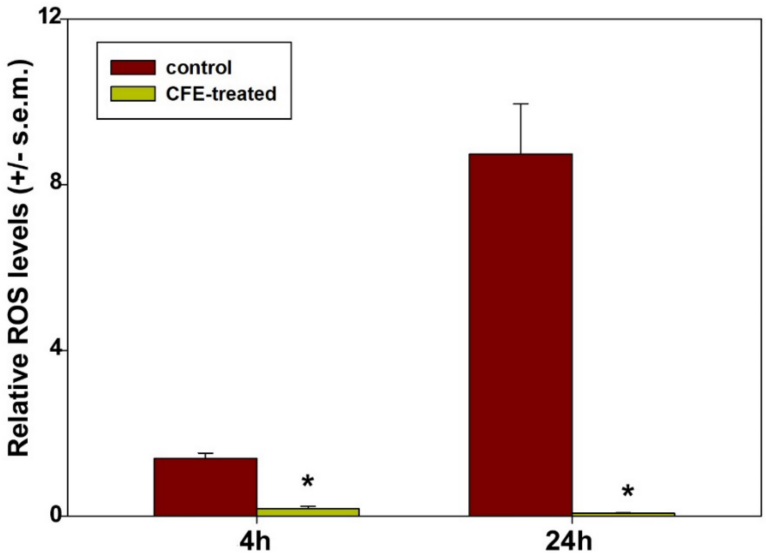

Figure 7. Bar graphs showing the ROS^+ cell/ROS^- cell ratio in control and $IC_{50}24$ CFE-treated HepG2 cells for 4 and 24 h. The error bars correspond to the standard error of the mean (s.e.m.) of three independent measurements. * $p < 0.05$.

In order to determine whether the CFE could affect the autophagic behavior of HepG2 cells, acridine orange staining was performed to label AVOs, a hallmark of autophagic cells that is indicative of autophagosome accumulation and autolysosome formation [31], at early (4 h of exposure) and late (24 h of exposure) time points. As shown in Figure 8, in this case, two distinct cell subpopulations characterized by low (AVO^-) and high rate (AVO^+) of acridine orange fluorescence were found after the flow cytometric assays and plot analyses. The present data confirmed that HepG2 cells are characterized by a high basal level of autophagy, as already indicated in [23,32]. In fact, the percentage of AVO^+ cells accounted for about 90% and 70% at 4 and 24 h of culture under control conditions. Conversely, the percentage of AVO^+ cells decreased after 4 h of treatment with $IC_{50}24$ CFE to about 70%, and the prolongation of the time of exposure to 24 h determined the complete disappearance of the AVO^+ cell fraction, whose proportion dropped to about 0.2% of the total population.

In order to verify to what extent inhibition of the autophagic process could be responsible for the observed CFE-dependent cytotoxicity on HepG2 cells, cells were co-incubated with $IC_{50}24$ CFE and 1 nM rapamycin (sirolimus), a known inhibitor of mTOR (mammalian target of rapamycin) serine/threonine protein kinase, which acts as autophagy promoter. As shown in Figure 9, this co-treatment was unable to reverse the CFE-triggered decrease in cell number, thereby suggesting the occurrence of extensive and widespread damage induced by exposure to CFE.

Lastly, we examined the effect of the incubation with $IC_{50}24$ CFE from A. lixula on HepG2 cells' migratory ability through a scratch wound healing assay. As expected, based on some previously published results [23,33,34], the panel of micrographs in Figure 10 shows that control HepG2 cells exhibited a locomotory attitude that determined the reduction in the denuded area (mean area % = 23 at time 0), which had already started at 2 h from the scratch time (mean area % = 17) and led to its partial obliteration after 6 h (mean area % = 6) and total closure within 22 h. Notably, since the doubling time of HepG2 cells is $\geq$24 h [35,36], the observed effect could not be ascribable to cell proliferation. In contrast, the exposure to the CFE inhibited the cells' ability to migrate into the scratched area and, in addition, starting from 2 h of exposure and in line with the previous data, the cells displayed prominent signs of suffering and damage, such as rounding and clumping, ultimately determining their visible detachment from the substrate.

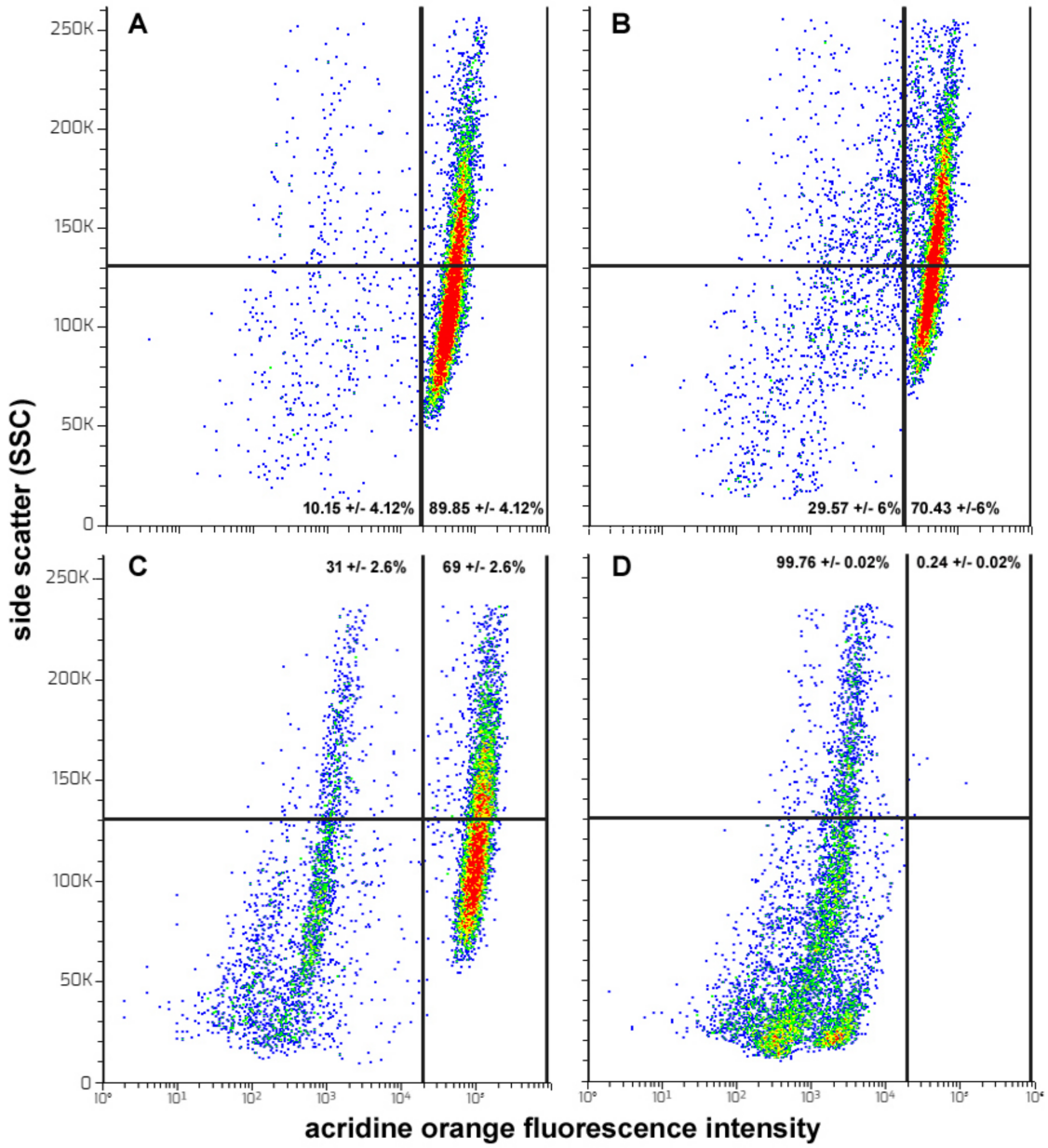

Figure 8. Flow cytometric assays for AVO accumulation in HepG2 cells grown under control conditions for 4 h (**A**) and 24 h (**C**) or incubated with IC_{50}24 CFE for 4 h (**B**) and 24 h (**D**). The plots show the results of representative experiments, and the percentages indicated as the mean ± s.e.m. of three independent experiments refer to AVO^+ cells (right quadrants) and AVO^- cells (left quadrants).

In light of the observed cytotoxic role played by the CFE from A. lixula on HepG2 tumor cells, proteomic analysis of the preparations was performed after proteolysis of the samples and MS sequencing to detect bioactive components. Overall, 1952 obtained spectra matched forward peptides, and the final output reported 104 forward and 20 reverse proteins and 329 unique forward peptides. The estimated spectrum-level FDR on true proteins was 0.3%. A bioinformatic similarity search against the BlastP database identified 28 proteins contained in the CFE and potentially associated with the various aspects related to the derangement of HepG2 cell biological activities reported previously here, as well as with exosome secretion. The peptide sequences and the results of alignments selected on the basis of sorting by the best E value are reported in Table 1.

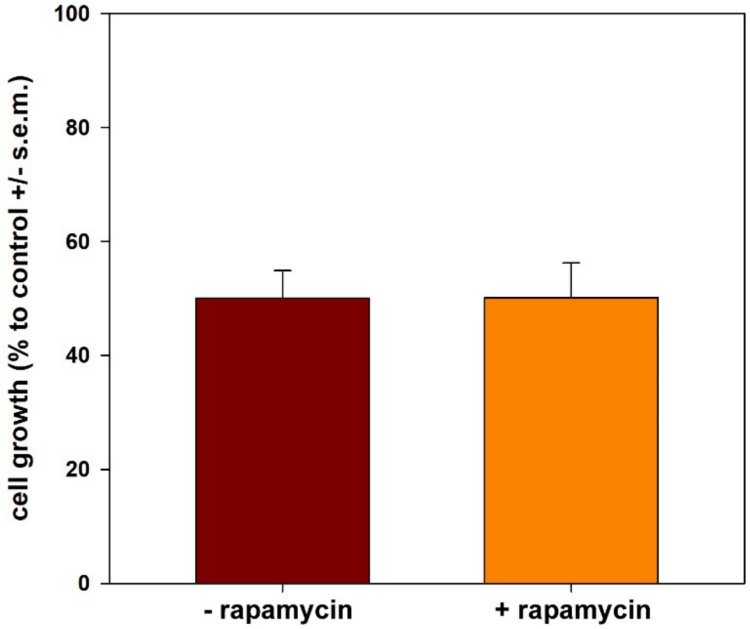

Figure 9. Bar graphs showing the absence of a statistically significant effect by 1 nM rapamycin co-treatment on CFE-induced decrease in cell number after 24 h of exposure. The error bars correspond to the standard error of the mean (s.e.m.) of three independent measurements.

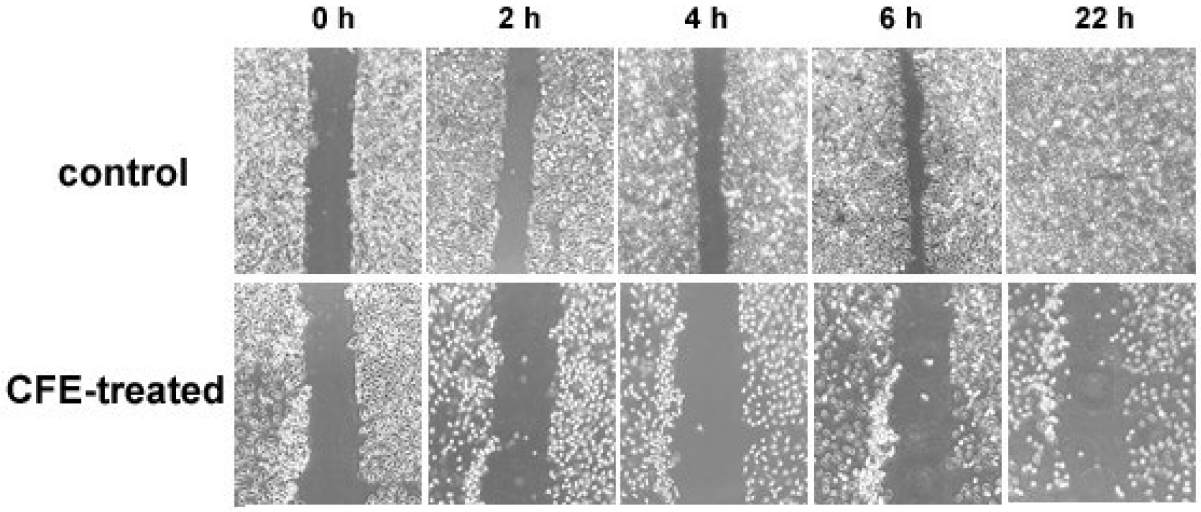

Figure 10. Panel of representative phase-contrast micrographs acquired during the wound healing assays at different time points under control conditions and in the presence of IC_{50}24 CFE. The assay was performed in triplicate. Microscopical magnification = 20×.

Table 1. Cytotoxic activity-associated protein profile of the CFE from *A. lixula*.

Peptide Sequence(s)	Sequence ID (nr. of Matches/Range)	Expected	Identities (%)	Positives (%)	Protein Description	Organism (Sea Urchin)	Selected GO Annotations
AIGNIGEPVER	BAL43173.1 (1/501–511)	2×10^{-7}	100		Apolipoprotein B-like protein, partial	*Mesocentrotus nudus*	-lipid transport
AAIQSMR	(1/543–549)	0.003	100	100			
LN [+0.984] QLHYLVGMEPSATDATVFLR				100			
AYTIDAQYK	(1/807–828)	5×10^{-19}	100	100			
LQSPMIK	(1/1069–1077)	1×10^{-5}	100	100			
QGITFNVFSSYPTLNK	(1/1815–1821)	0.12	88	88			
	(1/5231–5246)	9×10^{-13}	100	100			
LALIALK	BAL43173.1 (1/494–500)	0.021	100	100	Apolipoprotein B-like protein, partial	*Strongylocentrotus intermedius*	
NTLPTKDTIEQEK	AAC26833.1 (1/26–39)	1×10^{-7}	93	100	Thymosin beta	*Strongylocentrotus purpuratus*	-actin monomer binding -negative regulation of cell cycle G_1/S phase transition -regulation of cell migration
RGTIEVSKYDGSYR	XP_041457866.1 (1/572–584)	2×10^{-9}	100	100	Low-density lipoprotein receptor-related protein 1B-like	*Lytechinus variegatus*	-integral component of membrane -receptor-mediated endocytosis
GEQVYGITTYADTR	(1/725–738)	9×10^{-10}	94	93			
GNPTTVFPEIFK	XP_030853362.1 (1/206–217)	1×10^{-8}	100	100	Cryptochrome-2 isoform X1	*Strongylocentrotus purpuratus*	-circadian regulation of gene expression -DNA binding
	XP_030853363.1 (1/79–90)	1×10^{-8}	100	100	Cryptochrome-2 isoform X2		
TSPNSLEPSTTVLSPYLK	XP_030853362.1 (1/367–386)	1×10^{-14}	100	100	Cryptochrome-2 isoform X1		
	XP_030853363.1 (1/79–90) XP_030853362.1	1×10^{-14}	100	100	Cryptochrome-2 isoform X2		
VYSPIVFGK	(1/540–548)	2×10^{-4}	91	100	Cryptochrome-2 isoform X1		
	XP_030853363.1 (1/413–421)	2×10^{-4}	91	100	Cryptochrome-2 isoform X2		
LAAEGLR	XP_041456451.1 (1/62–68)	0.007	100	100	Arylsulfatase-like	*Lytechinus variegatus*	-sulfuric ester hydrolase activity -lysosome
IGTYGETR	XP_041464311.1 (1/109–118)	3×10^{-4}	100	100			
VFLPWTTTGLPK	XP_041460692.1 (1/146–157)	1×10^{-8}	100	100			
SLSWEGGHR	(1/352–360)	1×10^{-4}	91	100			

Table 1. *Cont.*

Peptide Sequence(s)	Sequence ID (nr. of Matches/Range)	Expected	Identities (%)	Positives (%)	Protein Description	Organism (Sea Urchin)	Selected GO Annotations
LVDGSSSNEGR		2×10^{-6}	100	100	Deleted in malignant brain tumors (DMBT) 1 protein isoform X1		
	XP_030831017.1, (20/25–35, 132–142, 239–249, 346–356, 453–463, 560–570, 667–677, 774–784, 881–891, 988–998, 1098–1108, 1353–1363, 1460–1470, 1567–1577, 1674–1684, 1781–1791, 1995–2005, 2102–2112, 2319–2329, 2426–2436)	2×10^{-6}	100	100	DMBT1 protein isoform X2		
	XP_030831023.1 (20/same as isoform X1 except for 1350–1360, 1457–1467, 1564–1574, 1671–1681, 1778–1788, 1992–2002, 2099–2109, 2316–2326, 2423–2433)	2×10^{-6}	100	100	DMBT1 protein isoform X3		
	XP_030831029.1 (20/same as isoform X2)	2×10^{-6}	100	100	DMBT1 protein isoform X9		
	XP_030831072.1 (19/same as isoform X1 without 2426–2436)		100				
	XP_030831034.1 (19/same as isoform X9 except for 1888–1898, 2212–2222, 2319–2329)	2×10^{-6}		100	DMBT1 protein isoform X4		
	XP_030831054.1 (19/same as isoform X9)	2×10^{-6}	100	100	DMBT1 protein isoform X7		
	XP_030831048.1 (19/same as isoform X4 except for 1995–2005)	2×10^{-6}	100	100	DMBT1 protein isoform X6		
	XP_030831064.1 (19/same as isoform X6 except for 991–1001, 1246–1256)		100				
	XP_030831041.1 (19/same as isoform X9 except for 2212–2222, 2319–2329)	$2e^{-6}$		100	DMBT1 protein isoform X8	*Strongylocentrotus purpuratus*	-membrane -scavenger receptor activity -endocytosis
	XP_030831078.1 (19/same as isoform X1 except for 1202–1212, 1309–1319, 1416–1426, 1523–1533, 1630–1640, 1844–1854, 1951–1961, 2166–2176, 2275–2285)	2×10^{-6}	100	100	DMBT1 protein isoform X5		
	XP_030831079.1 (19/same as isoform X9 except for 2209–2219)	2×10^{-6}	100		DMBT1 protein isoform X10		
	XP_030831086.1 (17/25–35, 132–142, 239–249, 346–356, 453–463, 560–570, 667–677, 774–784, 988–998, 1095–1105, 1202–1212, 1309–1319, 1416–1426, 1630–1640, 1737–1747, 1954–1964, 2061–2071)	2×10^{-6}	100	100	DMBT1 protein isoform X11		
	XP_030834718.1 (1/278–289)	2×10^{-6}	100	100	DMBT1 protein isoform X12		
	XP_030855705.1 (1/677–687)						
MLGYNGALSAPR	(1/1259–1269)	5×10^{-6}	100	100			
LVGGSGPHEGR	(1/1917–1927)	0.27	69	76	DMBT1 protein-like		
	(1/2449–2459)	1×10^{-6}	100	100	DMBT1 protein		
	(1/2129–2139)	0.27	77	76			
	(1/1590–1600)	0.017	77	76			
	(1/2553–2563)	0.096	77	84			
	XP_030851619.1 (1/839–849)	0.19	77	76			
	(1/1443–1453)	0.78	69	69			
		0.49	85	100			
LVGGSNDADGR		0.061	92	100	DMBT1 protein-like		

Table 1. *Cont.*

Peptide Sequence(s)	Sequence ID (nr. of Matches/Range)	Expected	Identities (%)	Positives (%)	Protein Description	Organism (Sea Urchin)	Selected GO Annotations
VLEQSDLVVDNEYALYTLIQPK	XP_030847432.1 (1/183–192)	0.092	75	83	BTB/POZ domain-containing protein At2g30600	*Strongylocentrotus purpuratus*	-protein ubiquitination
MIFIQGFVPAGADR	CBX45521.1 (1/37–50)	3×10^{-11}	100	100	Galectin-8 protein	*Paracentrotus lividus*	-membrane -integrin binding
NLLSVAYK	XP_780530.1 (1/20–26)	0.35	100	100	14-3-3-like protein 2	*Strongylocentrotus purpuratus*	-signal transduction
RLVELINQ	XP_030850878.1 (1/715–722)	1×10^{-4}	100	100	Centrosomal protein of 85 kDa (CEP85) isoform X1	*Strongylocentrotus purpuratus*	-spindle pole -regulation of mitotic centrosome separation
VLAYNVFELR	XP_041469541.1 (1/103–112)	4×10^{-7}	100	100	Sphingomyelinase C 2-like	*Lytechinus variegatus*	- acid sphingomyelin phosphodiesterase activity
GDSTLQFKPK	XP_041482277.1 (1/359–368)	5×10^{-6}	100	100	Tripartite motif-containing protein 45-like	*Lytechinus variegatus*	-ubiquitin-protein transferase activity -zinc ion binding
RLITRNSYE KEEELES RAAQFAALM KHQSYNVAMEWANIV	XP_030831990.1 (1/1592–1600) (1/2501–2507) (1/2775–2783) (1/3026–3040)	4×10^{-6} 0.003 2×10^{-5} 2×10^{-13}	 100 100 	 100 100 	Chromodomain-helicase-DNA-binding protein 8	*Strongylocentrotus purpuratus*	binding -negative regulation of canonical Wnt signaling pathway
DN [+0.984] IVIGGQAGVYDPNR	XP_001198520.2 (1/164–179)	1×10^{-12}	100	100	Hemicentin-2	*Strongylocentrotus purpuratus*	-calcium ion binding -response to stimulus
RVASGPLGLI	XP_030854745.1 (1/1903–1912)	1×10^{-5}	100	1000	WD repeat-containing protein 81	*Strongylocentrotus purpuratus*	-cytoplasmic vesicle
QINLDLLR	XP_041482078.1 (1/665–674)	2×10^{-4}	100	100	TBC1 domain family member 2B-like isoform X1	*Lytechinus variegatus*	-activation of GTPase activity
YPHTQLISQMDR	XP_030846390.1 (1/372–383)	1×10^{-9}	100	100	Growth/differentiation factor 8-like	*Strongylocentrotus purpuratus*	-signaling receptor binding -negative regulation of skeletal muscle satellite cell proliferation
MQVQ [+0.984] SGVPK	XP_003726849.3 (1/1–9)	1×10^{-4}	100	100	Selenide, water dikinase	*Strongylocentrotus purpuratus*	-selenocysteine biosynthetic process
KYSEPTVEDISPVEHVE	XP_030841466.1 (1/132–148)	3×10^{-10}	100	100	Kv channel-interacting protein 4-like	*Strongylocentrotus purpuratus*	-potassium channel regulator activity -calcium ion binding
DFIVIQNFITEEEEDSLLK	XP_011661956.1 (1/144–162)	2×10^{-16}	100	100	Alpha-ketoglutarate-dependent dioxygenase alkB homolog 7, mitochondrial	*Strongylocentrotus purpuratus*	-mitochondrial matrix -regulation of mitochondrial membrane permeability involved in programmed necrotic cell death

Table 1. *Cont.*

Peptide Sequence(s)	Sequence ID (nr. of Matches/Range)	Expected	Identities (%)	Positives (%)	Protein Description	Organism (Sea Urchin)	Selected GO Annotations
REVPVASL	XP_011668608.2 (1/721–728)	0.001	100	100	Sterile alpha motif domain-containing protein 9-like	*Strongylocentrotus purpuratus*	-intracellular membrane-bounded organelle
LAKALQLSE	XP_030841717.1 (1/221–229)	0.003	91	90	Hematopoietically expressed homeobox protein HHEX homolog	*Strongylocentrotus purpuratus*	-Wnt signaling pathway -negative regulation of cyclin-dependent protein serine/threonine kinase activity
SQIPTK	XP_041485363.1 (1/1915–1920) XP_041485364.1 (1/1424–1431)	0.024 0.024	100 100	100 100	Methylcytosine dioxygenase TET3-like isoform X1 Methylcytosine dioxygenase TET3-like isoform X2	*Lytechinus variegatus*	-methylcytosine dioxygenase activity -chromatin organization
QVTGTGATGR GGSSAQAIR	XP_796458.1 (1/107–116) NP_999723.1 (1/36–44)	2×10^{-5} 4×10^{-4}	100 100	100 100	Histone H1, gonadal-like Histone H1-beta, late embryonic	*Strongylocentrotus purpuratus*	
HLQLAIR	XP_030843320.1 (1/83–89)	0.002	100	100	Histone H2A-like, partial	*Strongylocentrotus purpuratus*	
NDEELNKLLGGVTIAQGGVLPNIQAVLLPK	XP_001175793.2 (1/89–118)	6×10^{-26}	100	100	Histone H2A, embryonic-like		
KLLSGVTIAQGGVLPNIQAVLLPK	NP_999718.1 (1/97–119)	3×10^{-18}	100	100	Late histone H2A.L3		
GDEELDSLIK	NP_001116980.1 (1/93–102)	7×10^{-6}	100	100	Histone H2A.V		
RKESYGIYIYKV	P022892 (1/33–42)	0.002	100	100	Histone H2B, embryonic	*Strongylocentrotus purpuratus*	
VLK	(1/43–45)						
QVHPDTGISSR	(1/46–56)						
AMSIMNSFVNDVFER	NP_001229615.1 (1/56–70)	6×10^{-12}	100	100	Histone H2B-like		
STITSR	XP_030836142.1 (1/84–89)	0.10	100	100	Histone H2B		
IAAEASR	AAB48832.1 (1/75–81)	0.016	100	100	Cleavage stage histone H2B	*Psammechinus miliaris*	
RLLLPGELAKH	(102–110)	6×10^{-5}	100	100			
HAVSEGTK	(110–118)	0.002	100	100			
YRPGTVALR	XP_030830328.1 (1/42–50)	2×10^{-5}	100	100			
STELLIR	(1/58–64)	0.008	100	100			
EIAQDFKTELR	(1/74–84)	7×10^{-8}	100	100	Histone H3, embryonic-like	*Strongylocentrotus purpuratus*	
FQSSAVMALQEASEAYLVGLFEDTN							
[+0.984] LC [+57.021] AIH-AK	(1/85–112)	3×10^{-22}	94	93			
DNIQGITKPAIR	CAA75404.1 (1/1–12)	2×10^{-7}	100	100	Histone H4, partial	*Arbacia lixula*	
RISGLIYEETR	(1/22–32)	3×10^{-6}					
VFLENVIR	(1/37–44)	2×10^{-4}					
TLYGFGG	XP_011664585.2 (1/97–102)	0.051	100	100	Histone H4-like	*Strongylocentrotus purpuratus*	

4. Discussion

Sea urchins' coelomic fluid represents a pseudo-vascular system designed for the transport of nutrients and gases and the fulfillment of the immune defense and stress response reactions. It contains a complex mixture of soluble molecules secreted constitutively by different parts of the echinoderm's body, whose identification and biological characterization are still very limited. In terms of possible biomedical translation, the available literature data only indicated that the cell-free CF from Tripneustes depressus possessed anti-viral properties against Suid herpesvirus type I and rabies virus, whereas that of Echinometra mathaei was endowed with a high radical-scavenging activity [37,38]. Additional studies focused on the characterization of protein components in the CFEs from different echinoderm species, pointing them out as potential sources of anti-microbial and anti-cancer agents [19,39]. Interestingly, D'Alessio et al. [40] recently found the presence of exosome-like extracellular vesicles in Strongylocentrotus purpuratus's CF and characterized their associated protein cargo, thus suggesting an increasing complexity in the composition of the fluid.

Previous results had revealed for the first time the beneficial effects of A. lixula's CFE against human triple-negative breast cancer, using MDA-MB231 cells as a model system [20]. In this case, the biological characterization of the cytotoxic activity highlighted the arrest of the cells in the S phase of the cell cycle, the depolarization of the mitochondria and the up-regulation of ROS production, although no occurrence of apoptotic death and of modification in AVOs' accumulation rate was observed.

Here we focused our attention on determining the possible protective effects exerted by the extract against the HepG2 cell line selected as an in vitro model of cancer of the digestive system, i.e., hepatocellular carcinoma. This aggressive neoplastic histotype represents the most common form of primary liver cancer, ranking sixth in incidence and fourth in mortality among all tumors [41]. Although hepatocarcinogenesis is multifactorial, the main risk factors include chronic fibrosing liver disease and cirrhosis [42]. Within the altered microenvironment of chronic liver injury, the damaged hepatocytes are addressed to a sustained regeneration program coupled with liver progenitor cell expansion, which ultimately results in the accumulation of genetic alterations and progressive cell de-differentiation likely responsible for their neoplastic transformation [43]. The advances in the knowledge of the major molecular signaling pathways involved in the development of hepatocellular carcinoma (HCC) prompted the analysis of the potential preventive and therapeutic roles of natural products, able to intervene in the modulation of the oncogenesis-linked intracellular events [44,45]. However, an accurate biological characterization of the molecular mechanism of action of the agents under study is the essential foundation for the successful development of targeted treatments.

Our data depicted an anti-HCC role of the CFE preparation, at least under the conditions used, but displaying different characteristics from those reported for breast carcinoma cells. In fact, exposure of HepG2 cells to the extract determined cell addressing to the sub-G_0 phase after arrest at the G_2/M phase associated with apoptotic death that reached massive completion after 48 h. During this time, cells underwent gradual mitochondrial depolarization and ROS and AVO depletion. Consistent with the derangement of cells' healthy state, an early block of cells' motile activities was also demonstrated, thus suggesting that the CFE may also act as a potential suppressor of HCC metastatic ability. The panel of study endpoints chosen to test the efficacy of the CFE on HCC cells provides a framework of phenotypic changes that converge to confirm its powerful inhibitory effect.

As a complement to the study of the effect of CFE treatment on cell phenotype, we undertook a search at the proteomic level of CFE's molecular constituents that may conceivably be involved in the observed cytotoxic activity. This study predicted a number of putative anti-cancer proteins responsible for the lethal effect on HepG2 cells. In addition, as already reported for Holothuria tubulosa's CFE [23], histones, which can be considered exosome-linked signatures, were also detected, suggesting the release of extracellular vesicles carrying, among the others, the intracellular constituents likely causing the anti-

HepG2 effects. It is known that extracellular histones are involved in exosome-mediated adhesion and could conceivably be involved in exosome uptake by target cells and the subsequent activation of signaling [46]. Exosomes are conceivably preserved intact by the method of preparation of the CFE and, therefore, could be ready to fuse with and transfer their cargo into cancer cells. In addition, to strengthen our hypothesis, Tadayoni Nia et al. [47] reported that the siRNA-mediated silencing of the gene coding for the transmembrane WD repeat-containing protein 81, one of the protein signatures found in our analysis, was able to reduce the release of exosomes by human glioblastoma cells.

Among the protein signatures identified, most of them may be mainly, but not exclusively, associated with the activation of programmed cell death. Lipid-free apolipoprotein B has been shown to exert cytotoxic effects on several cytotypes through binding and disturbing the structure of their plasmalemma, thereby triggering apoptosis [48]. The early report by Hall [49] ascribed to thymosin β10 an apoptosis-controlling role by functioning as an actin-mediated tumor suppressor, which induces cytoskeletal disorganization. In addition, Thr^{20} was found to be specifically required for actin sequestration and apoptosis promotion in ovarian cancer cells, whose thymosin-dependent inhibition of the Ras pathway was acknowledged [50,51]. Arylsulfatases are common components of toxic secretions of different animal organisms [52]; of note, Lai et al. [53] reported the effect of the up-regulation of SULF1, coding for arylsulfatase-1, on the decrease in the proliferation rate and motile attitude in vitro and tumorigenesis in vivo of liver tumor cell lines, and the potentiation of cell sensitivity to apoptotic stimuli possibly via inhibition of both the MAP kinase/ERK and PI3 kinase/AKT kinase pathways. Deleted In Malignant Brain Tumors 1 (DMBT1), which was also found in the CFE of Holothuria tubulosa [23], acts as a tumor growth suppressor and an effector of genetic resistance to liver carcinogenesis in rats and humans [54]. Its overexpression in GBC-SD gallbladder cancer cells was proven to decrease cell proliferation rate and induce apoptosis via stabilization of the phosphatase and tensin homolog (PTEN) and inhibition of the PI3K-Akt pathway, also reducing xenograft tumor growth in vivo [55]. BTB/POZ domain-containing proteins were found to inhibit proliferation, locomotion and invasion; impair cell cycle; and promote apoptosis in a panel of different tumor cell lines, also restraining xenograft tumor growth [56–58]. Hadari et al. [59] demonstrated that the integrin-binding protein galectin-8 was responsible for the inhibition of the adhesion of human lung cancer cells to the substrate, thereby addressing them to apoptosis. Autelli et al. [60] produced evidence that the increase of intracellular ceramide generated by acid sphingomyelinase-mediated sphingomyelin cleavage determined the activation of caspases and the stimulation of the intrinsic pathway of apoptosis in rat hepatoma cells co-treated with TNF and cycloheximide. Tripartite motif-containing protein 45 is a tumor suppressor member of the RING-finger-containing E3 ligases. Data from Peng et al. [61] and Zhang et al. [62] demonstrated its ability to promote cell apoptosis by activating the p38 signal and inhibit proliferation by down-regulating p-ERK in lung cancer cells, as well as to suppress glioblastoma proliferation and tumorigenicity by protecting p53 from degradation and inactivation, thereby allowing cells to undergo apoptosis. The inhibition of the intrinsic pathway of apoptosis was a result of the absence of functioning growth/differentiation factor 8, a.k.a. myostatin, in knockout C2C12 cells; the same factor was also proven to reduce the viability and disrupt the migratory and proliferative potential of MCF-7 breast cancer cells [63,64]. Ultimately, sterile alpha motif domain-containing protein 9 was reported to play a fundamental role in the interferon β-induced apoptotic pathway in human glioblastoma cells [65].

In addition, some protein signatures may be mainly associated with the impairment of the cell cycle and the inhibition of cell proliferation. This is the case of 14-3-3 protein, CEP85, cryptochrome-2, chromodomain-helicase-DNA-binding protein 8, HHEX, low-density lipoprotein receptor-related protein 1B and TET3 [66–74]. In particular, the p53-inducible oncosuppressor 14-3-3 is known to prevent the import of the cyclin B1/cdc2 complex in the nucleus and to bind to CDK2 and CDK4, thus likely affecting the G_1/S transition. Overexpression of CEP85 was found responsible for preventing centrosome

disjunction during mitosis. Knockdown of cryptochrome-2, a core component of the circadian clock, was proven to up-regulate osteosarcoma cell proliferation and migration by inducing cell cycle progression and promoting the MAPK and Wnt/β-catenin signaling pathways; similarly, chromodomain-helicase-DNA-binding protein 8 also functions as a tumor suppressor by regulating Wnt/β-catenin signaling and the cell cycle. Overexpressed HHEX was reported to restrain hyperproliferation, metabolism activity, cell size and transformation characteristic of c-Myc tumorigenic activities by binding and breaking c-Myc/Max heterodimers; in particular, dealing with liver cancer, HHEX proved capable of inhibiting tumorigenicity of Hepa1-6 hepatoma cells by suppressing their growth and colony-forming ability in vitro and tumor development in nude mice. Overexpression of full-length LRP1B, coding for the low-density lipoprotein receptor-related protein 1B, led to an impaired proliferation of human non-small cell lung cancer cells, whereas its knockdown exerted the opposite effect. In addition, this protein was found to function as a tumor suppressor also against renal cell cancer, its down-regulation leading to the increase in cell migration and invasion, possibly via actin cytoskeleton remodeling regulated through the Cdc42/RhoA pathway and expressional alteration of the components of focal adhesion complexes. Ultimately, a knockdown of the expression of TET3 was reported to promote the proliferation of HepG2 cells.

One of the identified protein signatures, i.e., alkB homolog 7, could be associated with mitochondrial damage. In fact, data from Fu et al. [75] demonstrated its involvement in the massive loss of mitochondrial homeostasis leading to permeability transition pore opening, NAD^+ efflux into the cytoplasm and, eventually, energy depletion and cellular demise.

Regarding the four remaining signatures listed, it may be inferred that: (i) selenide and water dikinase determine the decrease in ROS accumulation since Na et al. [76] reported that deficient cells showed the down-regulation of genes involved in ROS scavenging; (ii) Kv channel-interacting protein 4 acts as a putative tumor suppressor, as shown in hepatocellular carcinoma [77]; (iii) hemicentin-1 acts as putative cytotoxicity-associated factor, as shown in breast cancer [78]; and, (iv) TBC1 domain family member 2B, a Rab22-binding protein, is an inhibitor of cell motile attitude by blocking E-cadherin degradation necessary for epithelial-mesenchymal transition, as demonstrated with human lung cancer cells [79].

By taking the obtained results and the literature data into consideration, the findings reported here allow us to make the following comments:

(1) For HepG2 cells, anti-cancer agent-triggered growth arrest at the G_2/M phase is an event commonly leading up to apoptosis. This impairment was ascribed to different causes, such as the inhibition of cyclin-dependent kinase-2A, the activation of p38 MAPK signalization or the inhibition of tubulin polymerization, determining the failure of the assembly and dynamics of mitotic spindle structure [80–82]. Therefore, the molecular basis of CFE-stimulated cell cycle block is an interesting aspect that remains to be clarified and can bring to light new intracellular targets for anti-HCC treatment options;

(2) It is known that HepG2 cells are endowed with elevated levels of basal autophagy [23,56]. This allows their survival, active growth and locomotion by fulfilling the related high metabolic and energetic demands. Thus, it is conceivable that the suppression of "protective" autophagy may contribute to CFE's cytotoxic activity. Interestingly, in line with [83], autophagy down-regulation may lead to the inhibition of cell proliferation and the onset of apoptosis via the intrinsic pathway, as suggested in our model system by the derangement of mitochondrial function. On the other hand, the failure of rapamycin co-treatment to restore cell viability suggests that autophagy inhibition is secondary to the other CFE exposure-linked aspects of cell damage, i.e., mitochondrial dysfunction, ROS depletion and apoptosis promotion, the latter determining a massive impairment of cell functions that cannot be rescued by the sole autophagy reactivation;

(3) It is worth mentioning that the HepG2 cell line is characterized by low levels of expression of the cytochrome P450 family 2 subfamily E member 1 (CYP2E1) protein,

a ROS-generating enzyme of the endoplasmic reticulum, and therefore is considered a helpful model to test the formation of ROS mainly from mitochondrial sources [84]. Our results show a drastic reduction in the generation of mitochondrial ROS in exposed cells. It is known that low levels of ROS act as redox-active signaling messengers necessary for cell proliferation and functions and that cancer cells require a greater supply of these molecules; otherwise, they become unable to grow normally [85]. Thus, by analogy with the literature data, it is conceivable that the redox imbalance occurring in CFE-treated HepG2 cells may also contribute to the cytotoxicity-leading vicious cycle by promoting mitochondrial dysfunction and triggering mitochondria-mediated apoptosis.

A limitation of this study is represented by the lack of identification of the "active constituent(s)" of the CFE responsible for the death-promoting activity. Our results indicate that this (these) compound(s) withstand(s) lyophilization, resuspension and freeze–thawing cycles. Nevertheless, the proteomic profile analysis revealed the presence of a rich mix of proteins that can seemingly play anti-cancer roles at different levels. Moreover, molecular docking analyses by Wydananda et al. [39] also demonstrated the potential of peptides from A. lixula's CF to act as anti-non small cell lung cancer agents due to their ability to inhibit different signaling pathways implicated in the progression of this tumoral histotype. Thus, cumulative evidence prompts focusing attention on the protein components of the CFE for a future and more detailed examination of their biological properties and possible applications.

5. Conclusions

Overall, our results provide evidence for the cytotoxic potential of A. lixula's CFE against HCC cells, which comes in addition to the anti-triple negative breast cancer effect previously published [Luparello], thus increasing the interest in the biomedical implementation of the preparation. Future work will focus on the isolation of the substance(s) responsible for the cytotoxic effect and on the more detailed characterization of the underlying molecular mechanism(s) that mediate(s) cell death. Given the great need for developing alternative treatment options against liver cancer, our results indicate that the aqueous extract of A. lixula's CF can be taken into consideration as a potential anti-HCC agent for the development of novel prevention and/or treatment agents, which could also be included as a supplement in functional food or during food processing and packaging.

Author Contributions: Conceptualization, C.L., V.A. and M.V.; investigation, R.B., G.A., V.L., S.S. and M.M.; data curation, C.L., S.S., V.D.S. and M.V.; writing—original draft preparation, C.L. and M.V.; writing—review and editing, C.L. and M.V.; supervision, C.L., V.A. and M.V.; funding acquisition, C.L. and M.V. All authors have read and agreed to the published version of the manuscript.

Funding: This research was funded by The University of Palermo (Italy), grant Fondo Finalizzato alla Ricerca (FFR) 2021, to C.L. and M.V.

Institutional Review Board Statement: The "Assessorato regionale dell'agricoltura, sviluppo rurale e pesca mediterranea" of Sicily has approved the use of A. lixula in this study (authorization nr. 87468 of 25 October 2021).

Informed Consent Statement: Not applicable.

Data Availability Statement: The data presented in the current study are available from the corresponding author upon request.

Conflicts of Interest: The authors declare no conflict of interest.

References

1. Li, C.Q.; Ma, Q.Y.; Gao, X.Z.; Wang, X.; Zhang, B.L. Research Progress in Anti-Inflammatory Bioactive Substances Derived from Marine Microorganisms, Sponges, Algae, and Corals. *Mar. Drugs* **2021**, *19*, 572. [CrossRef] [PubMed]
2. Lindequist, U. Marine-Derived Pharmaceuticals? *Challenges and Opportunities. Biomol. Therap.* **2016**, *24*, 561–571. [CrossRef]

3. Liu, L.; Zheng, Y.Y.; Shao, C.L.; Wang, C.Y. Metabolites from marine invertebrates and their symbiotic microorganisms: Molecular diversity discovery, mining, and application. *Mar. Life Sci. Technol.* **2019**, *1*, 60–94. [CrossRef]
4. Lazzara, V.; Arizza, V.; Luparello, C.; Mauro, M.; Vazzana, M. Bright Spots in The Darkness of Cancer: A Review of Starfishes-Derived Compounds and Their Anti-Tumor Action. *Mar. Drugs* **2019**, *17*, 617. [CrossRef] [PubMed]
5. Luparello, C.; Mauro, M.; Lazzara, V.; Vazzana, M. Collective Locomotion of Human Cells, Wound Healing and Their Control by Extracts and Isolated Compounds from Marine Invertebrates. *Molecules* **2020**, *25*, 2471. [CrossRef]
6. Luparello, C.; Mauro, M.; Arizza, V.; Vazzana, M. Histone Deacetylase Inhibitors from Marine Invertebrates. *Biology* **2020**, *9*, 429. [CrossRef]
7. Mauro, M.; Lazzara, V.; Punginelli, D.; Arizza, V.; Vazzana, M. Antitumoral compounds from vertebrate sister group: A review of Mediterranean ascidians. *Dev. Comp. Immunol.* **2020**, *108*, 103669. [CrossRef]
8. Luparello, C. Marine Animal-Derived Compounds and Autophagy Modulation in Breast Cancer Cells. *Foundations* **2021**, *1*, 3–20. [CrossRef]
9. Šimat, V.; Elabed, N.; Kulawik, P.; Ceylan, Z.; Jamroz, E.; Yazgan, H.; Čagalj, M.; Regenstein, J.M.; Özogul, F. Recent Advances in Marine-Based Nutraceuticals and Their Health Benefits. *Mar. Drugs* **2020**, *18*, 627. [CrossRef]
10. Debeaufort, F. Active biopackaging produced from by-products and waste from food and marine industries. *FEBS Open Bio* **2021**, *11*, 984–998. [CrossRef]
11. Lobine, D.; Rengasamy, K.R.R.; Mahomoodally, M.F. Functional foods and bioactive ingredients harnessed from the ocean: Current status and future perspectives. *Crit. Rev. Food Sci. Nutr.* **2021**, *16*, 5794–5823. [CrossRef] [PubMed]
12. Wangensteen, O.S.; Turon, X.; Pérez-Portela, R.; Palacín, C. Natural or naturalized? Phylogeography suggests that the abundant sea urchin Arbacia lixula is a recent colonizer of the Mediterranean. *PLoS ONE* **2012**, *7*, e45067. [CrossRef] [PubMed]
13. Cakal Arslan, O.; Parlak, H. Embryotoxic effects of nonylphenol and octylphenol in sea urchin Arbacia lixula. *Ecotoxicol.* **2007**, *6*, 439–444. [CrossRef] [PubMed]
14. Carballeira, C.; De Orte, M.R.; Viana, I.G.; Delvalls, T.A.; Carballeira, A. Assessing the toxicity of chemical compounds associated with land-based marine fish farms: The sea urchin embryo bioassay with Paracentrotus lividus and Arbacia lixula. *Arch. Environ. Contam. Toxicol.* **2012**, *2*, 249–261. [CrossRef] [PubMed]
15. Vazzana, M.; Mauro, M.; Ceraulo, M.; Dioguardi, M.; Papale, E.; Mazzola, S.; Arizza, V.; Beltrame, F.; Inguglia, L.; Buscaino, G. Underwater high frequency noise: Biological responses in sea urchin Arbacia lixula (Linnaeus, 1758). *Comp. Biochem. Physiol. A Mol. Integr. Physiol.* **2020**, *242*, 110650. [CrossRef]
16. Cirino, P.; Brunet, C.; Ciaravolo, M.; Galasso, C.; Musco, L.; Vega Fernández, T.; Sansone, C.; Toscano, A. The Sea Urchin Arbacia lixula: A Novel Natural Source of Astaxanthin. *Mar. Drugs* **2017**, *15*, 187. [CrossRef]
17. Galasso, C.; Orefice, I.; Toscano, A.; Vega Fernández, T.; Musco, L.; Brunet, C.; Sansone, C.; Cirino, P. Food Modulation Controls Astaxanthin Accumulation in Eggs of the Sea Urchin Arbacia lixula. *Mar. Drugs* **2018**, *16*, 186. [CrossRef]
18. Stabili, L.; Acquaviva, M.I.; Cavallo, R.A.; Gerardi, C.; Narracci, M.; Pagliara, P. Screening of Three Echinoderm Species as New Opportunity for Drug Discovery: Their Bioactivities and Antimicrobial Properties. *Evid. Based Complement. Alternat. Med.* **2018**, *2018*, 7891748. [CrossRef]
19. Sciani, J.M.; Emerenciano, A.K.; Cunha da Silva, J.R.; Pimenta, D.C. Initial peptidomic profiling of Brazilian sea urchins: Arbacia lixula, Lytechinus variegatus and Echinometra lucunter. *J. Venom Anim. Toxins Incl. Trop. Dis.* **2016**, *22*, 17. [CrossRef]
20. Luparello, C.; Ragona, D.; Asaro, D.M.L.; Lazzara, V.; Affranchi, F.; Arizza, V.; Vazzana, M. Cell-Free Coelomic Fluid Extracts of the Sea Urchin Arbacia lixula Impair Mitochondrial Potential and Cell Cycle Distribution and Stimulate Reactive Oxygen Species Production and Autophagic Activity in Triple-Negative MDA-MB231 Breast Cancer Cells. *J. Mar. Sci. Eng.* **2020**, *8*, 261. [CrossRef]
21. Donato, M.T.; Tolosa, L.; Gómez-Lechón, M.J. Culture and Functional Characterization of Human Hepatoma HepG2 Cells. *Methods Mol. Biol.* **2015**, *1250*, 77–93. [CrossRef] [PubMed]
22. European Medicines Agency. Comparability of Biotechnological/Biological Products Subject to Changes in Their Manufacturing Process. Available online: https://www.ema.europa.eu/en/documents/scientific-guideline/ich-q-5-e-comparability-biotechnological/biological-products-step-5_en.pdf (accessed on 20 November 2021).
23. Luparello, C.; Branni, R.; Abruscato, G.; Lazzara, V.; Drahos, L.; Arizza, V.; Mauro, M.; Di Stefano, V.; Vazzana, M. Cytotoxic capability and the associated proteomic profile of cell-free coelomic fluid extracts from the edible sea cucumber Holothuria tubulosa on HepG2 liver cancer cells. *EXCLI J.* **2022**, *21*, 722–743. [CrossRef] [PubMed]
24. Longo, A.; Librizzi, M.; Chuckowree, I.S.; Baltus, C.B.; Spencer, J.; Luparello, C. Cytotoxicity of the urokinase-plasminogen activator inhibitor carbamimidothioic acid (4-boronophenyl) methyl ester hydrobromide (BC-11) on triple-negative MDA-MB231 breast cancer cells. *Molecules* **2015**, *20*, 9879–9889. [CrossRef]
25. Librizzi, M.; Longo, A.; Chiarelli, R.; Amin, J.; Spencer, J.; Luparello, C. Cytotoxic effects of Jay Amin hydroxamic acid (JAHA), a ferrocene-based class I histone deacetylase inhibitor, on triple-negative MDA-MB231 breast cancer cells. *Chem. Res. Toxicol.* **2012**, *25*, 2608–2616. [CrossRef] [PubMed]
26. Luparello, C.; Ragona, D.; Asaro, D.M.L.; Lazzara, V.; Affranchi, F.; Celi, M.; Arizza, V.; Vazzana, M. Cytotoxic Potential of the Coelomic Fluid Extracted from the Sea Cucumber Holothuria tubulosa against Triple-Negative MDA-MB231 Breast Cancer Cells. *Biology* **2019**, *8*, 76. [CrossRef]

27. Luparello, C.; Asaro, D.M.L.; Cruciata, I.; Hassell-Hart, S.; Sansook, S.; Spencer, J.; Caradonna, F. Cytotoxic activity of the histone deacetylase 3-selective inhibitor Pojamide on MDA-MB-231 triple-negative breast cancer cells. *Int. J. Mol. Sci.* **2019**, *20*, 804. [CrossRef]
28. Belyaeva, E.A.; Dymkowska, D.; Wieckowski, M.R.; Wojtczak, L. Reactive oxygen species produced by the mitochondrial respiratory chain are involved in Cd2+-induced injury of rat ascites hepatoma AS-30D cells. *Biochim. Biophys. Acta* **2006**, *1757*, 1568–1574. [CrossRef]
29. Raja, S.M.; Clubb, R.J.; Ortega-Cava, C.; Williams, S.H.; Bailey, T.A.; Duan, L.; Zhao, X.; Reddi, A.L.; Nyong, A.M.; Natarajan, A.; et al. Anticancer activity of Celastrol in combination with ErbB2-targeted therapeutics for treatment of ErbB2-overexpressing breast cancers. *Cancer Biol. Ther.* **2011**, *11*, 263–276. [CrossRef]
30. Chang, C.W.; Chen, Y.S.; Chou, S.H.; Han, C.L.; Chen, Y.J.; Yang, C.C.; Huang, C.Y.; Lo, J.F. Distinct subpopulations of head and neck cancer cells with different levels of intracellular reactive oxygen species exhibit diverse stemness, proliferation, and chemosensitivity. *Cancer Res.* **2014**, *74*, 6291–6305. [CrossRef]
31. Gibson, S.B. Chapter Thirteen - Investigating the Role of Reactive Oxygen Species in Regulating Autophagy. *Meth. Enzymol.* **2013**, *528*, 217–235. [CrossRef]
32. Sun, Y.; Zou, H.; Yang, L.; Zhou, M.; Shi, X.; Yang, Y.; Chen, W.; Zhao, Y.; Mo, J.; Lu, Y. Effect on the liver cancer cell invasion ability by studying the associations between autophagy and TRAP1 expression. *Oncol. Lett.* **2018**, *16*, 991–997. [CrossRef] [PubMed]
33. Xie, X.; Zhu, H.; Zhang, J.; Wang, M.; Zhu, L.; Guo, Z.; Shen, W.; Wang, D. Solamargine inhibits the migration and invasion of HepG2 cells by blocking epithelial-to-mesenchymal transition. *Oncol. Lett.* **2017**, *14*, 447–452. [CrossRef] [PubMed]
34. Zheng, J.; Shao, Y.; Jiang, Y.; Chen, F.; Liu, S.; Yu, N.; Zhang, D.; Liu, X.; Zou, L. Tangeretin inhibits hepatocellular carcinoma proliferation and migration by promoting autophagy-related BECLIN1. *Cancer Manag. Res.* **2019**, *11*, 5231–5242. [CrossRef] [PubMed]
35. Furth, E.E.; Sprecher, H.; Fisher, E.A.; Fleishman, H.D.; Laposata, M. An in vitro model for essential fatty acid deficiency: HepG2 cells permanently maintained in lipid-free medium. *J. Lipid Res.* **1992**, *33*, 1719–1726. [CrossRef]
36. Desquiret, V.; Loiseau, D.; Jacques, C.; Douay, O.; Malthièry, Y.; Ritz, P.; Roussel, D. Dinitrophenol-induced mitochondrial uncoupling in vivo triggers respiratory adaptation in HepG2 cells. *Biochim. Biophys. Acta* **2006**, *1757*, 21–30. [CrossRef]
37. Salas-Rojas, M.; Galvez-Romero, G.; Anton-Palma, B.; Acevedo, R.; Blanco-Favela, F.; Aguilar-Setién, A. The coelomic fluid of the sea urchin Tripneustes depressus shows antiviral activity against Suid herpesvirus type 1 (SHV-1) and rabies virus (RV). *Fish Shellfish Immunol.* **2014**, *36*, 158–163. [CrossRef]
38. Soleimani, S.; Mashjoor, S.; Mitra, S.; Yousefzadi, M.; Rezadoost, H. Coelomic fluid of Echinometra mathaei: The new prospects for medicinal antioxidants. *Fish Shellfish Immunol.* **2021**, *117*, 311–319. [CrossRef]
39. Widyananda, M.H.; Pratama, S.K.; Samoedra, R.S.; Sari, F.N.; Kharisma, V.D.; Ansori, A.N.M.; Antonius, Y. Molecular docking study of sea urchin (Arbacia lixula) peptides as multi-target inhibitor for non-small cell lung cancer (NSCLC) associated proteins. *J. Pharm. Pharmacogn. Res.* **2021**, *9*, 484–496.
40. D'Alessio, S.; Buckley, K.M.; Kraev, I.; Hayes, P.; Lange, S. Extracellular Vesicle Signatures and Post-Translational Protein Deimination in Purple Sea Urchin (Strongylocentrotus purpuratus) Coelomic Fluid-Novel Insights into Echinodermata Biology. *Biology* **2021**, *10*, 866. [CrossRef]
41. Ko, K.L.; Mak, L.Y.; Cheung, K.S.; Yuen, M.F. Hepatocellular carcinoma: Recent advances and emerging medical therapies. *F1000Research* **2020**, *9*, 620. [CrossRef]
42. Zimmermann, A. Etiology and Pathogenesis of Hepatocellular Carcinoma: Inflammatory and Toxic Causes. In *Tumors and Tumor-Like Lesions of the Hepatobiliary Tract: General and Surgical Pathology*; Zimmermann, A., Ed.; Springer International Publishing: Cham, Switzerland, 2017; pp. 2931–2959.
43. Wallace, M.C.; Friedman, S.L. Hepatic fibrosis and the microenvironment: Fertile soil for hepatocellular carcinoma development. *Gene Expr.* **2014**, *16*, 77–84. [CrossRef] [PubMed]
44. Alnajjar, A.M.; Elsiesy, H.A. Natural products and hepatocellular carcinoma: A review. *Hepatoma Res.* **2015**, *1*, 119–124. [CrossRef]
45. Jain, D.; Murti, Y.; Khan, W.U.; Hossain, R.; Hossain, M.N.; Agrawal, K.K.; Ashraf, R.A.; Islam, M.T.; Janmeda, P.; Taheri, Y.; et al. Roles of Therapeutic Bioactive Compounds in Hepatocellular Carcinoma. *Oxid. Med. Cell Longev.* **2021**, *2021*, 9068850. [CrossRef]
46. Singh, A.; Verma, S.; Modak, S.B.; Chaturvedi, M.M.; Purohit, J.S. Extra-nuclear histones: Origin, significance and perspectives. *Mol. Cell. Biochem.* **2022**, *477*, 507–524. [CrossRef]
47. Tadayoni Nia, A.; Bazi, Z.; Khosravi, A.; Oladnabi, M. WDR81 Gene Silencing Can Reduce Exosome Levels in Human U87-MG Glioblastoma Cells. *J. Mol. Neurosci.* **2021**, *71*, 1696–1702. [CrossRef]
48. Morita, S.Y.; Deharu, Y.; Takata, E.; Nakano, M.; Handa, T. Cytotoxicity of lipid-free apolipoprotein B. *Biochim. Biophys. Acta* **2008**, *1778*, 2594–2603. [CrossRef] [PubMed]
49. Hall, A.K. Thymosin beta-10 accelerates apoptosis. *Cell. Mol. Biol. Res.* **1995**, *41*, 167–180.
50. Rho, S.B.; Lee, K.W.; Chun, T.; Lee, S.H.; Park, K.; Lee, J.H. The identification of apoptosis-related residues in human thymosin beta-10 by mutational analysis and computational modeling. *J. Biol. Chem.* **2005**, *280*, 34003–34007. [CrossRef]
51. Lee, S.H.; Son, M.J.; Oh, S.H.; Rho, S.B.; Park, K.; Kim, Y.J.; Park, M.S.; Lee, J.H. Thymosin {beta}(10) inhibits angiogenesis and tumor growth by interfering with Ras function. *Cancer Res.* **2005**, *65*, 137–148. [CrossRef]

52. Rodrigo, A.P.; Mendes, V.M.; Manadas, B.; Grosso, A.R.; Alves de Matos, A.P.; Baptista, P.V.; Costa, P.M.; Fernandes, A.R. Specific Antiproliferative Properties of Proteinaceous Toxin Secretions from the Marine Annelid Eulalia sp. onto Ovarian Cancer Cells. *Mar. Drugs* **2021**, *19*, 31. [CrossRef]
53. Lai, J.P.; Yu, C.; Moser, C.D.; Aderca, I.; Han, T.; Garvey, T.D.; Murphy, L.M.; Garrity-Park, M.M.; Shridhar, V.; Adjei, A.A.; et al. SULF1 inhibits tumor growth and potentiates the effects of histone deacetylase inhibitors in hepatocellular carcinoma. *Gastroenterology* **2006**, *130*, 2130–2144. [CrossRef] [PubMed]
54. Frau, M.; Simile, M.M.; Tomasi, M.L.; Demartis, M.I.; Daino, L.; Seddaiu, M.A.; Brozzetti, S.; Feo, C.F.; Massarelli, G.; Solinas, G.; et al. An expression signature of phenotypic resistance to hepatocellular carcinoma identified by cross-species gene expression analysis. *Cell. Oncol.* **2012**, *35*, 163–173. [CrossRef] [PubMed]
55. Sheng, S.; Jiwen, W.; Dexiang, Z.; Bohao, Z.; Yueqi, W.; Han, L.; Xiaoling, N.; Tao, S.; Liu, H. DMBT1 suppresses progression of gallbladder carcinoma through PI3K/AKT signaling pathway by targeting PTEN. *Biosci. Biotechnol. Biochem.* **2019**, *83*, 2257–2264. [CrossRef] [PubMed]
56. Sun, G.; Peng, B.; Xie, Q.; Ruan, J.; Liang, X. Upregulation of ZBTB7A exhibits a tumor suppressive role in gastric cancer cells. *Mol. Med. Rep.* **2018**, *17*, 2635–2641. [CrossRef] [PubMed]
57. Xiang, T.; Tang, J.; Li, L.; Peng, W.; Du, Z.; Wang, X.; Li, Q.; Xu, H.; Xiong, L.; Xu, C.; et al. Tumor suppressive BTB/POZ zinc-finger protein ZBTB28 inhibits oncogenic BCL6/ZBTB27 signaling to maintain p53 transcription in multiple carcinogenesis. *Theranostics* **2019**, *9*, 8182–8195. [CrossRef] [PubMed]
58. He, J.; Wu, M.; Xiong, L.; Gong, Y.; Yu, R.; Peng, W.; Li, L.; Li, L.; Tian, S.; Wang, Y.; et al. BTB/POZ zinc finger protein ZBTB16 inhibits breast cancer proliferation and metastasis through upregulating ZBTB28 and antagonizing BCL6/ZBTB27. *Clin. Epigenetics* **2020**, *12*, 82. [CrossRef]
59. Hadari, Y.R.; Arbel-Goren, R.; Levy, Y.; Amsterdam, A.; Alon, R.; Zakut, R.; Zick, Y. Galectin-8 binding to integrins inhibits cell adhesion and induces apoptosis. *J. Cell Sci.* **2000**, *113*, 2385–2397. [CrossRef]
60. Autelli, R.; Ullio, C.; Prigione, E.; Crepaldi, S.; Schiavone, N.; Brunk, U.T.; Capaccioli, S.; Baccino, F.M.; Bonelli, G. Divergent pathways for TNF and C(2)-ceramide toxicity in HTC hepatoma cells. *Biochim. Biophys. Acta* **2009**, *1793*, 1182–1190. [CrossRef]
61. Peng, X.; Wen, Y.; Zha, L.; Zhuang, J.; Lin, L.; Li, X.; Chen, Y.; Liu, Z.; Zhu, S.; Liang, J.; et al. TRIM45 Suppresses the Development of Non-small Cell Lung Cancer. *Curr. Mol. Med.* **2020**, *20*, 299–306. [CrossRef]
62. Zhang, J.; Zhang, C.; Cui, J.; Ou, J.; Han, J.; Qin, Y.; Zhi, F.; Wang, R.F. TRIM45 functions as a tumor suppressor in the brain via its E3 ligase activity by stabilizing p53 through K63-linked ubiquitination. *Cell Death Dis.* **2017**, *8*, e2831. [CrossRef]
63. Wallner, C.; Drysch, M.; Becerikli, M.; Jaurich, H.; Wagner, J.M.; Dittfeld, S.; Nagler, J.; Harati, K.; Dadras, M.; Philippou, S.; et al. Interaction with the GDF8/11 pathway reveals treatment options for adenocarcinoma of the breast. *Breast* **2018**, *37*, 134–141. [CrossRef]
64. Drysch, M.; Schmidt, S.V.; Becerikli, M.; Reinkemeier, F.; Dittfeld, S.; Wagner, J.M.; Dadras, M.; Sogorski, A.; von Glinski, M.; Lehnhardt, M.; et al. Myostatin Deficiency Protects C2C12 Cells from Oxidative Stress by Inhibiting Intrinsic Activation of Apoptosis. *Cells* **2021**, *10*, 1680. [CrossRef] [PubMed]
65. Tanaka, M.; Shimbo, T.; Kikuchi, Y.; Matsuda, M.; Kaneda, Y. Sterile alpha motif containing domain 9 is involved in death signaling of malignant glioma treated with inactivated Sendai virus particle (HVJ-E) or type I interferon. *Int. J. Cancer* **2010**, *126*, 1982–1991. [CrossRef] [PubMed]
66. Kuroda, Y.; Aishima, S.; Taketomi, A.; Nishihara, Y.; Iguchi, T.; Taguchi, K.; Maehara, Y.; Tsuneyoshi, M. 14-3-3sigma negatively regulates the cell cycle, and its down-regulation is associated with poor outcome in intrahepatic cholangiocarcinoma. *Hum. Pathol.* **2007**, *38*, 1014–1022. [CrossRef] [PubMed]
67. Chen, C.; Tian, F.; Lu, L.; Wang, Y.; Xiao, Z.; Yu, C.; Yu, X. Characterization of Cep85 - a new antagonist of Nek2A that is involved in the regulation of centrosome disjunction. *J. Cell Sci.* **2015**, *128*, 3290–3303. [CrossRef] [PubMed]
68. Yu, Y.; Li, Y.; Zhou, L.; Yang, G.; Wang, M.; Hong, Y. Cryptochrome 2 (CRY2) Suppresses Proliferation and Migration and Regulates Clock Gene Network in Osteosarcoma Cells. *Med. Sci. Monit.* **2018**, *24*, 3856–3862. [CrossRef]
69. Sawada, G.; Ueo, H.; Matsumura, T.; Uchi, R.; Ishibashi, M.; Mima, K.; Kurashige, J.; Takahashi, Y.; Akiyoshi, S.; Sudo, T.; et al. CHD8 is an independent prognostic indicator that regulates Wnt/β-catenin signaling and the cell cycle in gastric cancer. *Oncol. Rep.* **2013**, *30*, 1137–1142. [CrossRef]
70. Su, J.; You, P.; Zhao, J.P.; Zhang, S.L.; Song, S.H.; Fu, Z.R.; Ye, L.W.; Zi, X.Y.; Xie, D.F.; Zhu, M.H.; et al. A potential role for the homeoprotein Hhex in hepatocellular carcinoma progression. *Med. Oncol.* **2012**, *29*, 1059–1067. [CrossRef]
71. Marfil, V.; Blazquez, M.; Serrano, F.; Castell, J.V.; Bort, R. Growth-promoting and tumourigenic activity of c-Myc is suppressed by Hhex. *Oncogene* **2015**, *34*, 3011–3022. [CrossRef]
72. Ni, S.; Hu, J.; Duan, Y.; Shi, S.; Li, R.; Wu, H.; Qu, Y.; Li, Y. Down expression of LRP1B promotes cell migration via RhoA/Cdc42 pathway and actin cytoskeleton remodeling in renal cell cancer. *Cancer Sci.* **2013**, *104*, 817–825. [CrossRef]
73. Beer, A.G.; Zenzmaier, C.; Schreinlechner, M.; Haas, J.; Dietrich, M.F.; Herz, J.; Marschang, P. Expression of a recombinant full-length LRP1B receptor in human non-small cell lung cancer cells confirms the postulated growth-suppressing function of this large LDL receptor family member. *Oncotarget* **2016**, *7*, 68721–68733. [CrossRef] [PubMed]
74. Zhong, X.; Liu, D.; Hao, Y.; Li, C.; Hao, J.; Lin, C.; Shi, S.; Wang, D. The expression of TET3 regulated cell proliferation in HepG2 cells. *Gene* **2019**, *698*, 113–119. [CrossRef] [PubMed]

75. Fu, D.; Jordan, J.J.; Samson, L.D. Human ALKBH7 is required for alkylation and oxidation-induced programmed necrosis. *Genes Dev.* **2013**, *27*, 1089–1100. [CrossRef] [PubMed]
76. Na, J.; Jung, J.; Bang, J.; Lu, Q.; Carlson, B.A.; Guo, X.; Gladyshev, V.N.; Kim, J.; Hatfield, D.L.; Lee, B.J. Selenophosphate synthetase 1 and its role in redox homeostasis, defense and proliferation. *Free Radic. Biol. Med.* **2018**, *127*, 190–197. [CrossRef] [PubMed]
77. Zhang, L.; Rong, W.; Ma, J.; Li, H.; Tang, X.; Xu, S.; Wang, L.; Wan, L.; Zhu, Q.; Jiang, B.; et al. Comprehensive Analysis of DNA 5-Methylcytosine and N6-Adenine Methylation by Nanopore Sequencing in Hepatocellular Carcinoma. *Front. Cell. Dev. Biol.* **2022**, *10*, 827391. [CrossRef]
78. Zhang, Y.; Tong, G.H.; Wei, X.X.; Chen, H.Y.; Liang, T.; Tang, H.P.; Wu, C.A.; Wen, G.M.; Yang, W.K.; Liang, L.; et al. Identification of Five Cytotoxicity-Related Genes Involved in the Progression of Triple-Negative Breast Cancer. *Front. Genet.* **2022**, *12*, 723477. [CrossRef]
79. Manshouri, R.; Coyaud, E.; Kundu, S.T.; Peng, D.H.; Stratton, S.A.; Alton, K.; Bajaj, R.; Fradette, J.J.; Minelli, R.; Peoples, M.D.; et al. ZEB1/NuRD complex suppresses TBC1D2b to stimulate E-cadherin internalization and promote metastasis in lung cancer. *Nat. Commun.* **2019**, *10*, 5125. [CrossRef]
80. Fatahala, S.S.; Sayed, A.I.; Mahgoub, S.; Taha, H.; El-Sayed, M.-I.k.; El-Shehry, M.F.; Awad, S.M.; Abd El-Hameed, R.H. Synthesis of Novel 2-Thiouracil-5-Sulfonamide Derivatives as Potent Inducers of Cell Cycle Arrest and CDK2A Inhibition Supported by Molecular Docking. *Int. J. Mol. Sci.* **2021**, *22*, 11957. [CrossRef]
81. Han, Z.; Zhao, X.; Zhang, E.; Ma, J.; Zhang, H.; Li, J.; Xie, W.; Li, X. Resistomycin Induced Apoptosis and Cycle Arrest in Human Hepatocellular Carcinoma Cells by Activating p38 MAPK Pathway In Vitro and In Vivo. *Pharmaceuticals* **2021**, *14*, 958. [CrossRef]
82. Ren, Y.; Ruan, Y.; Cheng, B.; Li, L.; Liu, J.; Fang, Y.; Chen, J. Design, synthesis and biological evaluation of novel acridine and quinoline derivatives as tubulin polymerization inhibitors with anticancer activities. *Bioorg. Med. Chem.* **2021**, *46*, 116376. [CrossRef]
83. Zhu, C.; Zhao, M.; Fan, L.; Cao, X.; Xia, Q.; Zhou, J.; Yin, H.; Zhao, L. Chitopentaose inhibits hepatocellular carcinoma by inducing mitochondrial mediated apoptosis and suppressing protective autophagy. *Bioresour. Bioprocess.* **2021**, *8*, 4. [CrossRef]
84. Jiang, J.; Briedé, J.J.; Jennen, D.G.; Van Summeren, A.; Saritas-Brauers, K.; Schaart, G.; Kleinjans, J.C.; de Kok, T.M. Increased mitochondrial ROS formation by acetaminophen in human hepatic cells is associated with gene expression changes suggesting disruption of the mitochondrial electron transport chain. *Toxicol. Lett.* **2015**, *234*, 139–150. [CrossRef] [PubMed]
85. Liu, B.; Tan, X.; Liang, J.; Wu, S.; Liu, J.; Zhang, Q.; Zhu, R. A reduction in reactive oxygen species contributes to dihydromyricetin-induced apoptosis in human hepatocellular carcinoma cells. *Sci. Rep.* **2014**, *4*, 7041. [CrossRef] [PubMed]